ISSN 1070-3284, Russian Journal of Coordination Chemistry, 2021, Vol. 47, No. 9, pp. 646–652. © Pleiades Publishing, Ltd., 2021.

A 3,5-Connected 3D Nickel-Mixed Ligands Coordination Polymer with Selective Adsorption of Carbon Dioxide

J. A. Hua[a, b], Z. P. Duan[a], C. K. Gao[a], X. H. Xie[a], Z. P. Qiao[a], T. Q. Feng[a], and X. Ma[a, b, *]

[a] *Chemistry and Chemical Engineering Department, Taiyuan Institute of Technology, Taiyuan, 030008 P.R. China*

[b] *State Key Laboratory of Coordination Chemistry, Nanjing University, Nanjing, 210023 P.R. China*

**e-mail: maxiang@tit.edu.cn*

Received January 15, 2021; revised February 23, 2021; accepted February 24, 2021

Abstract—The gas adsorption is an important research field of coordination chemistry and bioinorganic chemistry, in which the selective absorption of CO_2 in the presence of N_2 is a challenge in these fields. A coordination polymer $[Ni_2(tib)_2(1,4\text{-}NDC)_2]\cdot 7H_2O$ (NTN) was synthetized by the reaction of the mixed ligands: 1,4-naphthalenedicarboxylic acid (1,4-H_2NDC) and 1,3,5-tris(1-imidazolyl) benzene (Tib) with Ni^{2+} under solvothermal conditions. X-ray single-crystal analysis (CIF file CCDC no. 2053530) results indicate that NTN possesses a supramolecular isomers with two-fold interpenetrating 3D frameworks with $\{4^2\cdot 6^5\cdot 8^3\}\{4^2\cdot 6\}$ topology. NTN is further characterized by powder IR spectroscopy, elemental analysis, X-ray diffraction, and thermogravimetric analysis. Notably, NTN possess an excellent selective CO_2 sorption property compared with N_2.

Keywords: Ni(II)-coordination polymer, mixed-ligand strategy, gas adsorption crystal structure analysis

DOI: 10.1134/S1070328421090049

INTRODUCTION

Coordination polymers (CPs) that are constructed from transition metal ions coordinated by organic ligands have been received more and more attentions, owing to their aesthetically fascinating topological structures and potential applications in fluorescence recognition properties [1–6], gas storage/separation [7, 8], catalysis [9–11], magnetism [12–14], etc. The application of CPs in gas adsorption/separation are of great significance in scientific research and industrial production [15–17]. CO_2 is very important in life system, and is involved in many life pathways, which the adsorption of CO_2 at the molecular level is becoming an important research area in coordination chemistry and bio-inorganic chemistry [18, 19]. However, since the non-polarity and low molecular weight of CO_2, it is difficult to be adsorbed by tranditional inorganic materials, for example activated carbon. Hence, the synthesis of new CPs in CO_2 adsorption is not only a hot spot, but also a great challenge [20, 21].

Nowadays, most of CPs are composed by one-pot reaction method, which only one ligand was used in the reaction. It will be very difficult to synthesize CPs accurately select relatively similar polarity substances, since the single action site of one-ligand CPs [22, 23]. Therefore, a mixed ligands strategy should be explored in composing the precise selective CPs to overcome the shortcomings [21, 24, 25]. In addition, the one-pot reaction process is affected sensitively by the type of organic ligands, which the coordination modes, functional groups, and substituents of the organic ligands can bring about consequential effects on the final structures and properties [26–29]. Furthermore, some reaction factors, for example the ratio of metal-ligand, solvent, temperature, pH and counter ions can also affect the final networks by varying aforementioned parameters with the same building units [30–33]. Hence, the search for the precise conditions in the mixed-ligand strategy is also an important task [34, 35].

Herein, one 3,5-connected 3D CP $[Ni_2(Tib)_2(1,4\text{-}NDC)_2]\cdot 7H_2O$ (NTN) was synthesized by reacting mixed-ligands 1,3,5-tris(1-imidazolyl)benzene (Tib) and 1,4-naphthalenedicarboxylic acid (1,4-H_2NDC) with $Ni(NO_3)_2$ under solvothermal conditions. The structure of NTN were characterized by X-ray single crystal analysis, IR spectroscopy, elemental, powder X-ray diffraction (PXRD) and thermogravimetric analyses (TGA). Notably, NTN shows an excellent selective CO_2 adsorption property compared to N_2.

EXPERIMENTAL

Materials and methods. Reagents used in this study were all of analytical grade, purchased from commercial suppliers and used as received unless otherwise stated. $Ni(NO_3)_2\cdot 6H_2O$, 1,3,5-tribromobenzene, imidazole, 1,4-H_2NDC, KOH, DMF, and CH_3OH

were purchased from Macklin reagent Inc. (P.R. China). The Tib ligand was synthesized according to the method reported previously [36, 37]. All the solutions were prepared with ultrapure water filtered through Milli-Q academic system.

Elemental analyses for C, H and N were performed on a Perkin-Elmer 240C Elemental Analyzer. FT-IR spectra were recorded in the range of 400–4000 cm^{-1} on a Bruker Vector 22 FT-IR spectrophotometer using KBr pellets. Powder X-ray diffraction (PXRD) measurements were carried out on a Bruker D8 Advance X-ray diffractometer using CuK_α radiation (λ = 1.5418 Å), in which the X-ray tube was operated at 40 kV and 40 mA. Thermogravimetric analysis (TGA) were performed on a Mettler-Toledo (TGA/DSC1) thermal analyser under the N_2 atmosphere with a heating rate of 10°C min^{-1}.

Synthesis. A mixture of Tib (8.2 mg, 0.03 mmol), 1,4-H_2NDC (6.5 mg, 0.03 mmol), $Ni(NO_3)_2{\cdot}6H_2O$ (14.6 mg, 0.05 mmol) were dissolved in DMF-CH_3OH–H_2O mixed solvent (8 mL, v : v : v = 1 : 1 : 2). The mixted suspension was sealed in Teflon-lined stainless steel container and heated at 140°C for 3 days. After being cooled to room temperature, green block crystals of NTN were obtained in 85% yield.

For $C_{54}H_{50}N_{12}O_{15}Ni_2$			
Anal. calcd., %	C, 52.97	H, 4.12	N, 13.73
Found, %	C, 52.93	H, 4.18	N, 13.76

IR (KBr pellet; ν, cm^{-1}): 3396 w, 3124 m, 1618 s, 1567 m, 1508 s, 1460 m, 1419 s, 1363 s, 1311 w, 1284 m, 1241 m, 1102 m, 1077 s, 1016 s, 937 m, 877 w, 834 s, 797 m, 754 w, 693 m, 656 s, 562 w.

X-ray crystallography. Intensity data were collected on a Bruker APEX-II CCD diffractometer with MoK_α monochromated radiation (λ = 0.71073 Å) at 296(2) K. The intensities were corrected by Lorentz polarization factors and multiscan absorption. The structure was solved by the direct method and refined by the full-matrix least-squares on F^2 using the SHELXTL-97 software [38]. Hydrogen atoms were added according to theoretical models. The maximum and minimum peaks on the final difference Fourier map are 3.712 and 1.550 e $Å^{-3}$. All of the non-hydrogen atoms were refined anisotropically. A summary of crystal data and structure refinement for NTN are provided in Table 1. Selected bond lengths and angles of NTN are listed in Table 2.

Detailed information has been deposited at the Cambridge Crystallographic Data Centre (CCDC no. 2053530; deposit@ccdc.cam.ac.uk or http://www.ccdc.cam.ac.uk).

Adsorption property. The CO_2 and N_2 adsorption properties of NTN were investigated as previous literature reports [35]. Briefly, the bulk sample of NTN for adsorption experiment was obtained by heating the fresh complexes at 473 K for 20 h under high vacuum to remove the free and coordinated water molecules. Then, the adsorption and desorption of carbon dioxide (CO_2) at 195 K and nitrogen (N_2) at 77 K were measured on the Belsorp-Max volumetric sorbometer from 0 to 1 atm. Each experiment was repeated three times to obtain reliable data.

RESULTS AND DISCUSSION

As shown in Fig. 1a, the results of X-ray single crystal structures indicate that the asymmetric unit of NTN is $[Ni_2(Tib)_2(1,4\text{-}NDC)_2]{\cdot}7H_2O$ and exhibits a distorted octahedral coordination geometry, in which Ni^{2+} ions are located in a six-coordinated environment comprising three carboxylate oxygen atoms (O(1), O(4C), O(4C)) of two 1,4-NDC ligands and three imidazole nitrogen atoms (N(1), N(3A), N(5B)) of three distinct Tib. The topological analysis is also carried out and the simplified overall structure of NTN is a 2-fold interpenetrated (3,5)-connected 2-nodal ttd net with the point symbol of $\{4^2{\cdot}6^5{\cdot}8^3\}\{4^2{\cdot}6\}$ (Fig. 1b). In detail, each 1,4-NDC employs two carboxylate groups in (κ^1)-(κ^2)-μ_2-1,4-NDC coordination mode to connect with two Ni^{2+} ions generating an 1D zigzag chain (Fig. 1c). Coordination modes of 1,4-NDC appeared in NTN. Meanwhile each Tib also acts as a tridentate linker to connect three Ni^{2+} ions generating an 1D ladder chain (Fig. 1d). On the whole, the Ni(II)-1,4-NDC and Ni(II)-Tib chains interact with each other resulting in the final 3D porous framework of NTN (Fig. 1e). The void space (0.26 × 0.19 nm in size) along the *b* axis in the 3D structure is large enough to accommodate another equivalent net to stabilize the whole structure (Figs. 1b, 1e). After the solvent molecules were removed from the channels, PLATON calculations show that the accessible volume increased to 3214.0 $Å^3$ (30.2%) per unit cell volume [39, 40].

Hitherto, there are two similar 3D CPs [Cd(Tib)(1,4-NDC)·H_2O·2DMF](C1) [41], and [Co(Tib)(1,4-NDC)·H_2O·2DMF] (C2) [42]. However, there are three differences between NTN and them. First, their crystallize are in different space groups: NTN belongs to a monoclinic $P2_1/c$ space group, while C1 is monoclinic with the space group of $P2_1/n$. Secondly, NTN is constructed by using Ni^{2+} ions, rather than Cd^{2+} in C1 or Co^{2+} in C2. Thirdly, there are free DMF molecules in both C1 and C2 but water molecules in NTN, which will have a great influence on gas adsorption properties.

TGA of NTN were carried out under N_2 atmosphere. As shown in Fig. 2a, the TGA curve of NTN shows a weight loss of 10.51% in the temperature range of 30–275°C corresponding to the release of lattice water molecules (calcd. 10.29%). Furthermore, the

Table 1. Crystal data and structure refinements for NTN

Parameter	Value
Empirical formula	$C_{54}H_{50}N_{12}O_{15}Ni_2$
Formula weight	1224.48
Crystal system	Monoclinic
Space group	$P2_1/c$
a, Å	10.422(7)
b, Å	24.356(18)
c, Å	13.068(10)
α, deg	90.00
β, deg	112.677(10)
γ, deg	90.00
V, Å^3	3060.7(4)
Z	2
ρ_{calcd}, g cm^{-3}	1.329
μ, mm^{-1}	0.687
F(000)	1268
R_{int}	0.0496
Observed reflections ($I \geq 2\sigma(I)$)	20645
Unique reflections	7008
Goodness-of-fit	1.112
R_1, wR_2 ($I \geq 2\sigma(I)$)	0.0596, 0.1735
R_1, wR_2 (all data)	0.0936, 0.1951
Large diff. peak and hole, e Å^{-3}	0.981 and −0.552

Table 2. Selected bond lengths (Å) and bond angles (deg) for NTN*

Bond	d, Å	Bond	d, Å
Ni(1)–O(1)	2.030(3)	Ni(1)–N(1)	2.118(3)
Ni(1)–N(5)$^{\#1}$	2.060(3)	Ni(1)–O(3)$^{\#3}$	2.119(3)
Ni(1)–N(3)$^{\#2}$	2.080(3)	Ni(1)–O(4)$^{\#3}$	2.206(3)
Angle	**ω, deg**	**Angle**	**ω, deg**
O(1)Ni(1)N(5)$^{\#1}$	108.73(13)	N(5)$^{\#1}$Ni(1)O(3)$^{\#3}$	93.07(12)
O(1)Ni(1)N(3)$^{\#2}$	88.99(13)	N(3)$^{\#2}$Ni(1)O(3)$^{\#3}$	90.50(12)
N(5)$^{\#1}$Ni(1)N(3)$^{\#2}$	95.12(13)	O(1)Ni(1)O(4)$^{\#3}$	97.20(11)
O(1)Ni(1)N(1)	88.45(13)	N(5)$^{\#1}$Ni(1)O(4)$^{\#3}$	153.50(12)
N(5)$^{\#1}$Ni(1)N(1)	90.36(13)	N(3)$^{\#2}$Ni(1)O(4)$^{\#3}$	90.58(11)
N(3)$^{\#2}$Ni(1)N(1)	174.45(13)	N(1)Ni(1)O(4)$^{\#3}$	84.86(11)
O(1)Ni(1)O(3)$^{\#3}$	158.15(12)	O(3)$^{\#3}$Ni(1)O(4)$^{\#3}$	60.96(10)

* Symmetry transformations used to generate equivalent atoms: $^{\#1}$ $-x+1, -y+1, -z+1$; $^{\#2}$ $x, y, z-1$; $^{\#3}$ $x+1, -y+1/2, z+1/2$.

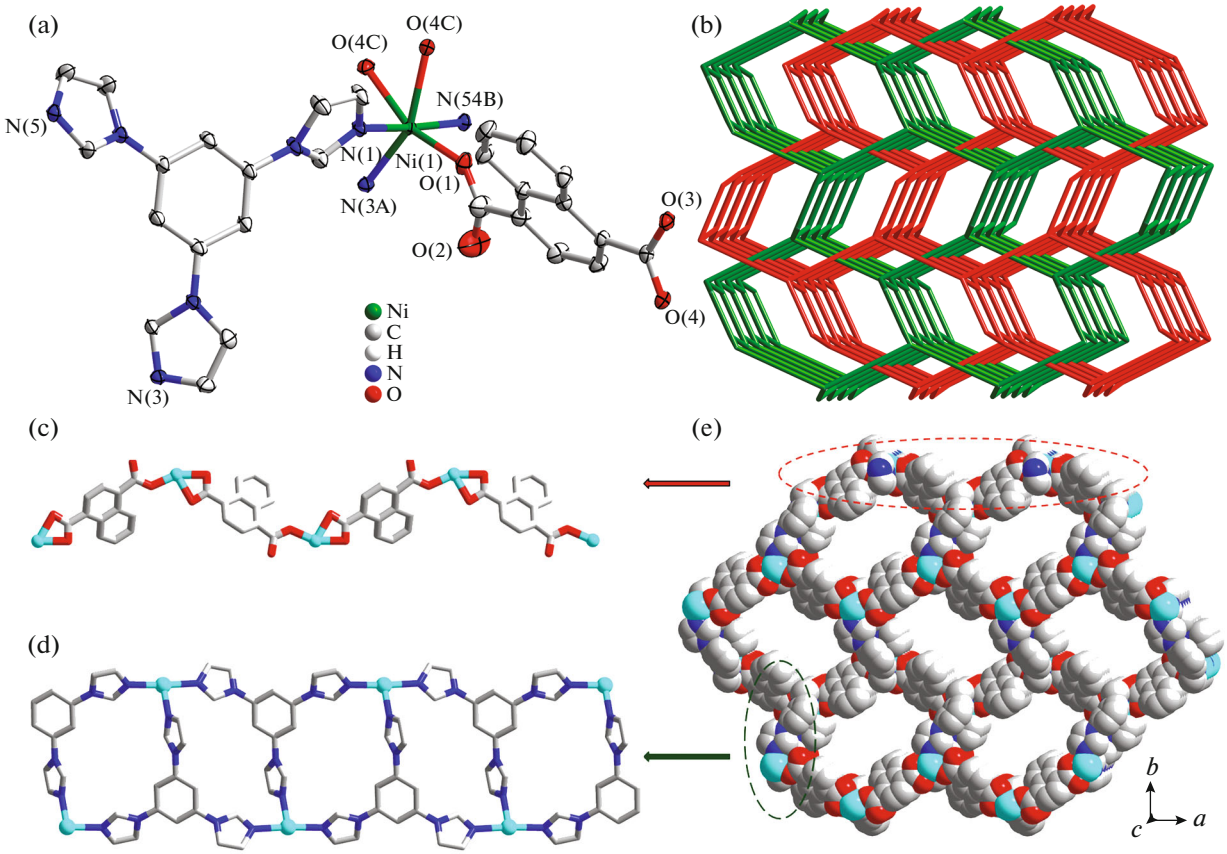

Fig. 1. Coordination environment of Ni(II) in NTN with the ellipsoids drawn at the 30% probability level. Hydrogen atoms and free water molecules are omitted for clarity (a); schematic representation of (3,5)-connected 2-fold interpenetrating ttd topology of NTN (b); 1D chain of Ni(II)-1,4-NDC (c); 1D chain of Ni(II)-Tib (d); schematic representation of 3D space-filling framework of NTN (e).

results indicate that the framework of NTN is stable up to about 360°C.

PXRD were performed with their bulk samples. As shown in Fig. 3, the as-synthesized PXRD patterns of NTN is in good agreement with its simulated ones, indicating phase purity of the samples. The desolvated samples of NTN were obtained by heating the as-synthesized samples at 200°C for 10 h under high vacuum. Then, the framework integrity was examined by PXRD. As shown in Fig. 3, the treated samples of NTN remain highly crystallized, and maintain the main framework features only with lost or shift of several peaks and occurrence of a few new peaks. This phenomenon may be probably origin from the distortion or shrinking of the crystal lattice due to heating and removal of guest molecules [42].

As shown in Fig. 3b, the TGA curve of treated NTN samples show a weight loss of about 4.52% in the temperature range of 30–200°C, corresponding to the release of three free water molecules (calcd. 4.68%). As shown in Fig. 4, in NTN, there are hydrogen bonds interact between some free water molecules or residue groups from the framework of NTN, for example O(1*w*) and O(2*w*), O(4*w*) and O(2). Both of them have shorter bond lengths and form strong hydrogen bonds, and hence these water molecules cannot be removed from the channels easily, even at 200°C [43, 44]. Moreover, the 2-fold interpenetrated factor can also prevent these molecules from releasing the framework [45, 46].

Gas adsorption properties were further measured with CO_2 or N_2 at 195 or 77 K, respectively. The activated samples of NTN were prepared by heating the as-synthesized samples at 200°C under vacuum for 10 h. As shown in Fig. 5, the CO_2 gas adsorption isotherm of NTN at 195 K shows a two-step curves with two abrupt jumps at $P \sim 0.005$ and 0.028 atm with notable hysteresis for desorption. When $P > 0.028$ atm, in the second step, the isotherm exhibits a sudden increase to 0.092 atm and then gradually attains saturation with the adsorbed CO_2 amount of 162.37 $cm^3\ g^{-1}$ (318.94 mg g^{-1}) at 1 atm, corresponding to 3.98 CO_2 molecules per formula unit. The Brunauer–Emmett–Teller (BET) surface area of NTN is about 434.76 $m^2\ g^{-1}$. The stepwise process and obvious hysteresis of CO_2 adsorption isotherm of treated samples

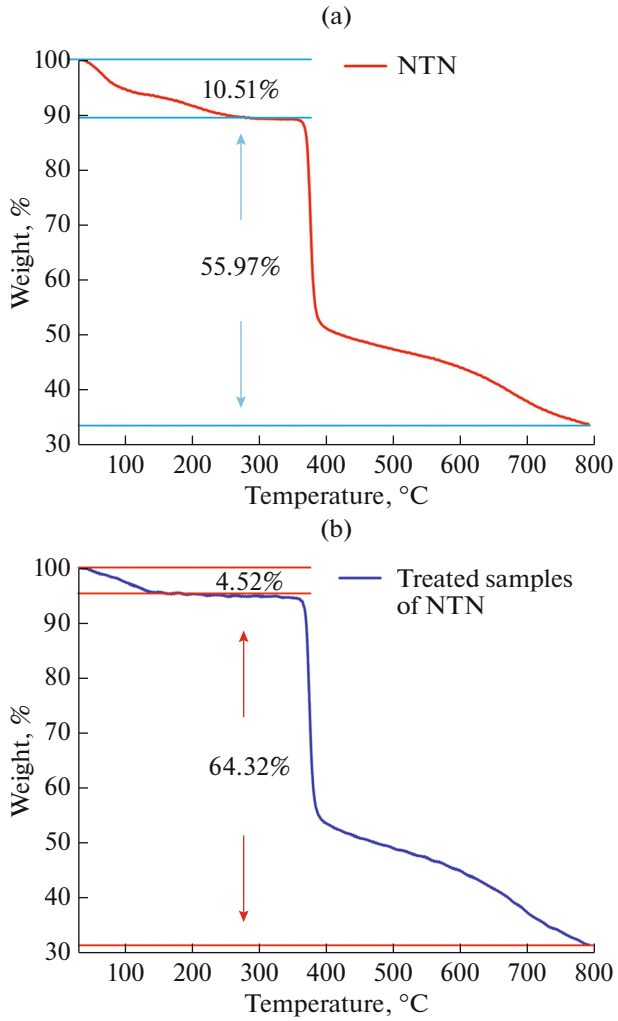

Fig. 2. The TGA curves of NTN (a) and treated samples of NTN (b).

of NTN may be attributed to the flexibility of the framework and the strong interactions between the framework and the guests or diffusion barrier hindering escape of the framework during the process of adsorption–desorption, and similar adsorption results were observed in previous reports [47–51].

As shown in Fig. 5, NTN has almost no adsorption on N_2 from 0 to 0.95 atm compared with CO_2. The selective CO_2 adsorption over N_2 observed for NTN may be partially attributed to the molecular size, since the smaller kinetic diameter of CO_2 is 3.30 Å compared to 3.64 Å of N_2. Hence, the diffusion rate of N_2 should be much slower in the 1D channel, which may result in no adsorption of N_2 at low temperature (77 K). Besides, the selectivity of CO_2 over N_2 can also be ascribed to the quadrupole–quadrupole interactions. In the skeleton of NTN, one carboxylate group of 1,4-NDC adopts a monodentate mode, in which only one O atom of the carboxylate group takes part in

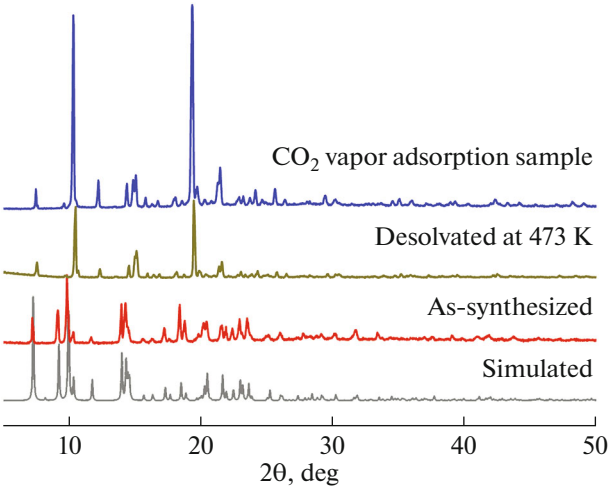

Fig. 3. PXRD patterns of NTN.

the coordination with metal centers. The other O atom is located on the wall of the porous surface, which the exposed O donors on the pore walls may interact effectively with quadrupole molecules. It can induce strong interactions between the framework and CO_2 molecules since its much larger quadrupole moment (-1.4×10^{-39} C m^2) than N_2 (-4.7×10^{-40} C m^2). These results may indicate that NTN is a promising material for selective adsorption of CO_2 from natural gas.

In this work, we have successfully synthesized a 3D coordination polymer (CP) $[Ni_2(Tib)_2(1,4\text{-}NDC)_2]\cdot 7H_2O$ by mixed-ligand strategy. NTN was characterized by X-ray single crystal analysis, IR spectrum, powder X-ray diffraction and thermogravimetric analysis. The results indicated that the coordination mode of the mixed-ligands play important roles in the construction of CP with structural diversification for NTN generating 3D network with $\{4^2\cdot6^5\cdot8^3\}\{4^2\cdot6\}$ topology. Furthermore, the mixture ligands endows NTN with excellent frame structure and floor area ratio in the gas adsorption. Moreover, the pore size of NTN enables it to selectively adsorb CO_2 compared with N_2. Hence, this work will be helpful for the design and synthesis of such selective adsorption structure compounds in the future.

FUNDING

This work was supported by the Natural Science Foundation of China (grant 21573056), Shanxi Province Science Foundation for Youths (grant 201901D211453), the Research Foundation of the Chinese State Key Laboratory of Coordination Chemistry (SKLCC1912), and the Scientific and Technological Innovation Programs of Higher Education Institutions in Shanxi (STIP 2020L0644).

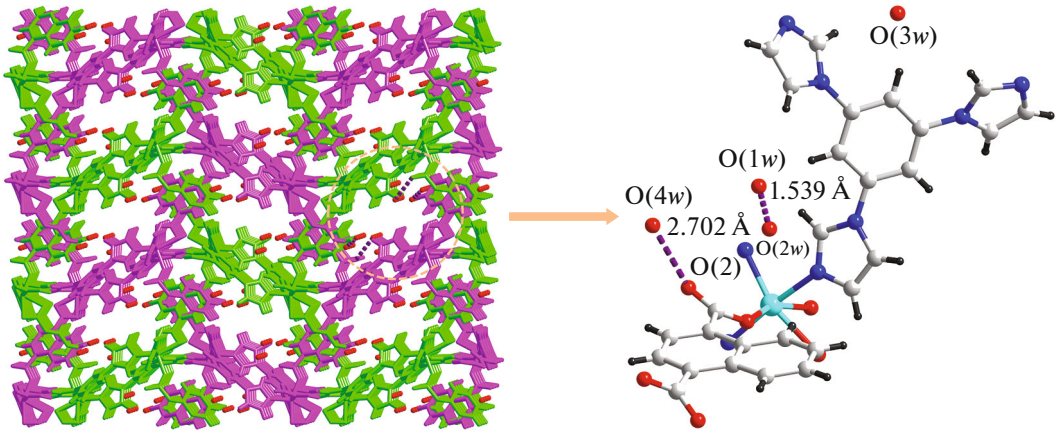

Fig. 4. The schematic representation of the strong hydrogen bonds between the free water molecules and frameworks in NTN.

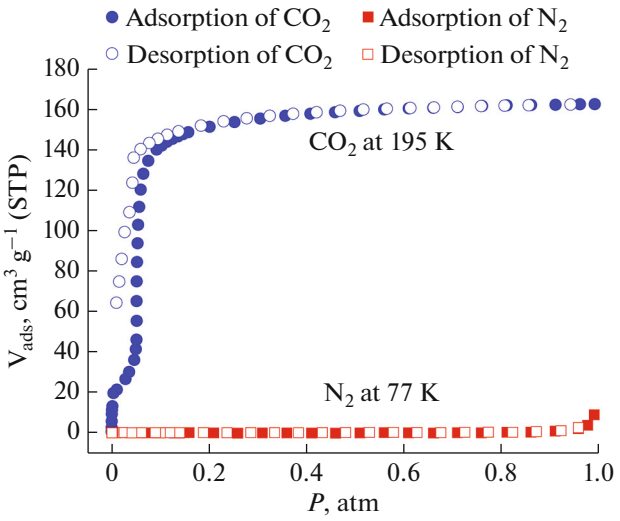

Fig. 5. Gas adsorption isotherms of NTN for CO_2 (195 K) and N_2 (77 K): filled shape, adsorption; open shape, desorption.

CONFLICT OF INTEREST

The authors declare that they have no conflicts of interest.

AUTHOR CONTRIBUTIONS

Author contributions X. Ma and J.A. Hua conceived the idea of the research. X. Ma and J.A. Hua designed the molecule, and J.A. Hua and Z.P. Duan synthesized the molecule. X. Ma, C.K. Gao and X.H. Xie designed and conducted the experiments. J.A. Hua, Z.P. Qiao and T.Q. Feng analyzed the data. All authors wrote and reviewed the manuscript.

REFERENCES

1. Zhao, D., Liu, X.H., Zhao, Y., et al., *J. Mater. Chem. A.*, 2017, vol. 5, p. 15797.
2. Hua, J.A., Zhou, Y.J., Bian, Y.J., et al., *J. Coord. Chem.*, 2020, vol. 73, p. 282.
3. Liu, G.L., Qin, Y.J., Jing, L., et al., *Chem. Commun.*, 2013, vol. 49, p. 1699.
4. Sun, C., Wang, X.L., Qin, C., et al., *Chem. Eur. J.*, 2013, vol. 19, p. 3639.
5. Rachuri, Y., Bisht, K.K., Suresh, E., et al., *Cryst. Growth Des.*, 2014, vol. 14, p. 3300.
6. Rachuri, Y., Parmar, B., Bisht, K., et al., *Dalton Trans.*, 2017, vol. 46, p. 3623.
7. Kitagawa, S. and Uemura, K., *Chem. Soc. Rev.*, 2005, vol. 34, p. 109.
8. Li, J.R., Kuppler, R.J., and Zhou, H.C., *Chem. Soc. Rev.*, 2009, vol. 38, p. 1477.
9. Kitagawa, S., Kitaura, R., and Noro, S., *Angew. Chem., Int. Ed.*, 2004, vol. 43, p. 2334.
10. Ma, L.Q., Abney, C., and Lin, W.B., *Chem. Soc. Rev.*, 2009, vol. 38, p. 1248.
11. Ma, X., Zhou, Y.J., Yuan, X.R., et al., *Inorg. Nano-Met. Chem.*, 2021, vol. 51, p. 332.
12. Zeng, Y.F., Hu, X., Liu, F.C., et al., *Chem. Soc. Rev.*, 2009, vol. 38, p. 469.
13. Polyzou, C.D. and Tangoulis, V., *J. Coord. Chem.*, 2019, vol. 72, p. 389.
14. Zhang, S.W. and Cheng, P., *Chem. Rec.*, 2016, vol. 16, p. 2077.
15. Lapshin, D.N., Jorge, M., Campbell, E.E.B., et al., *J. Mater. Chem. A.*, 2020, vol. 8, p. 11781.
16. Li, J.R., Kupplera, R.J., and Zhou, H.C., *Chem. Soc. Rev.*, 2009, vol. 38, p. 1477.
17. Ho, T.A., Wang, Y.F., and Criscenti, L.J., *Phys. Chem. Chem. Phys.*, 2018, vol. 20, p. 12390.
18. Sharma, A., Malani, A., Medhekar, N.V., et al., *CrystEngComm*, 2017, vol. 19, p. 6950.
19. Pham, K.D., Ly, T.H., Vu, T.V., et al., *New J. Chem.*, 2020, vol. 44, p. 18763.
20. Singh, G., Lee, J., Bahadur, A.R., et al., *Chem. Soc. Rev.*, 2020, vol. 49, p. 4360.
21. Lysova, A.A., Samsonenko, DG., Dorovatovskii, P.V., et al., *J. Am. Chem. Soc.*, 2019, vol. 141, p. 17260.

22. Zhang, S.-W., Shi, W., and Cheng, P., *Coord. Chem. Rev.*, 2017, vol. 352, p. 108.
23. Sapianik, A.A. and Fedin, V.P., *Russ. J. Coord. Chem.*, 2020, vol. 46, p. 443. https://doi.org/10.1134/S1070328420060093
24. Park, I.H., Mulijanto, C.E., Lee, H.H., et al., *Cryst. Growth & Des.*, 2016, vol. 16, p. 2504.
25. Liu, D., Chang, Y.J., and Lang, J.P., *CrystEngComm*, 2011, vol. 13, p. 1851.
26. Zhang, J.P., Zhang, Y.B., Lin, J.B., et al., *Chem. Rev.*, 2012, vol. 112, p. 1001.
27. Hua, J.A., Zhao, Y., Kang, Y.S., et al., *Dalton Trans.*, 2015, vol. 44, p. 11524.
28. Hua, J.A., Zhao, Y., Zhao, D., et al., *RSC Adv.*, 2015, vol. 5, p. 43268.
29. Ma, X., Zhao, Q., Wang, B., et al., *J. Mol. Struct.*, 2020, vol. 1206, p. 127714.
30. Fang, S.M., Zhang, Q., Hu, M., et al., *Inorg. Chem.*, 2010, vol. 49, p. 9617.
31. Niu, J.Y., Hua, J.A., Ma, X., et al., *CrystEngComm*, 2012, vol. 14, p. 4060.
32. Ma, X., Li, S.Z., Hua, J.A., et al., *J. Coord. Chem.*, 2013, vol. 66, p. 725.
33. Dybtsev, D.N., Samsonenko, D.G., and Fedin, V.P., *Russ. J. Coord. Chem.*, 2016, vol. 42, p. 557. https://doi.org/10.1134/S1070328416090013
34. Zhang, X.D., Hua, J.A., Guo, J.H., et al., *J. Mater. Chem. C.*, 2018, vol. 6, p. 12623.
35. Li, B., Yan, Q.Q., Xu, Z.Q., et al., *CrystEngComm*, 2020, vol. 22, p. 506.
36. Zhao, W., Song, Y., Okamura, T., et al., *Inorg. Chem.*, 2015, vol. 44, p. 3330.
37. Fan, J., Sun, W.Y., Okamura, T., et al., *Inorg. Chem.*, 2003, vol. 42, p. 3168.
38. Sheldrick, G.M. *SHEXTL-97, Programs for Crystal Structure Refinement*, Göttingen: Univ. of Göttingen, 1997.
39. Hua, J.A., Yuan, X., Ma, X., et al., *CrystEngComm*, 2020, vol. 22, p. 7832.
40. Ma, X., Wang, Y.Q., Hua, J.A., et al., *Sci. China. Chem.*, 2020, vol. 63, p. 73.
41. Xue, Z.Z., Sheng, T.L., Wang, Y.L., et al., *CrystEng-Comm*, 2015, vol. 17, p. 2004.
42. Yang, L., Cao, L., Li, X., et al., *Dalton Trans.*, 2017, vol. 46, p. 7567.
43. Aijaz, A., Sannudo, E.C., and Bharadwaj, P.K., *Cryst. Growth Des.*, 2011, vol. 11, p. 1122.
44. Singh, D. and Baruah, J.B., *Cryst. Growth Des.*, 2012, vol. 12, p. 2109.
45. Ji-Ai Hua, Yue Zhao, Qing Liu, Dan Zhao, Kai Chena, and Wei-Yin Sun, *CrystEngComm*, 2014, vol. 16, p. 7536.
46. Sun, D., Han, L.L., Yuan, S., et al., *Cryst. Growth Des.*, 2013, vol. 13, p. 377.
47. Maji, T.K., Uemura, K., and Chang, H.-C., *Angew. Chem., Int. Ed.*, 2004, vol. 43, p. 3269.
48. Park, H.J. and Suh, M.P., *Chem. Commun.*, 2010, vol. 46, p. 610.
49. Hou, C., Liu, Q., Lu, Y., et al., *CrystEngComm*, 2012, vol. 14, p. 8569.
50. Zhang, K., Lively, R.P., Dose, M.E., et al., *Chem. Commun.*, 2013, vol. 49, p. 3245.
51. Liu, B., Li, Y.P., Hou, L., et al., *J. Mater. Chem. A.*, 2013, vol. 1, p. 6535.